

The effect of thermal motion on the electron
localization in metal-to-ligand charge transfer
excitations in $[\text{Fe}(\text{bpy})_3]^{2+}$

Alex Domingo¹, Carmen Sousa², and Coen de Graaf^{3,4}

¹Department of Chemistry, KU Leuven, Celestijnenlaan 200F, B-3001
Heverlee-Leuven, Belgium

²Departament de Química Física and Institut de Química Teòrica i
Computacional, Universitat de Barcelona, C/ Martí i Franquès 1, 08028
Barcelona, Spain

³Departament de Química Física i Inorgànica, Universitat Rovira i
Virgili, Marcel·lí Domingo s/n, 43007 Tarragona, Spain.

⁴Institució Catalana de Recerca i Estudis Avançats (ICREA), Passeig
Lluís Companys 23, 08010, Barcelona, Spain

September 26, 2014

Abstract

Accurate electronic structure calculations of the lowest excited states have been performed on twenty snapshots of a molecular dynamics simulation of $[\text{Fe}(\text{bpy})_3]^{2+}$ dissolved in water. The thermal motion distorts the structure of the complex from its average D_3 symmetry, causing the localization on one bipyridine ligand of the excited electron in the metal-to-ligand charge transfer (MLCT) state. The excitation energy is about 0.25 eV lower than for the delocalized description of the MLCT state and is in good agreement with experiment. The composition of the MLCT band is carefully analyzed and the effect of the thermal motion on the mechanism of the light-induced spin crossover is discussed.

1 Introduction

The iron trisbipyridine complex $[\text{Fe}(\text{bpy})_3]^{2+}$ plays a central role in the elucidation of the light-induced excited spin state trapping (LIESST) process. Both from the experimental and the theoretical side, the complex received a great deal of attention and numerous studies have been published about the deactivation dynamics of the singlet metal-to-ligand charge transfer ($^1\text{MLCT}$) state.^{1–12} From these studies it became clear that after the initial excitation into the $^1\text{MLCT}$, the system reaches the meta-stable high-spin state (^5T) within approximately 130 fs and turns back to the initial low-spin state (^1A) after 650 ps.¹³ The deactivation from $^1\text{MLCT}$ to ^5T goes through an intersystem crossing in the CT manifold, populating the $^3\text{MLCT}$ state in an ultrafast process of approximately 30 fs. From there, it was thought that the system evolves directly to the final HS state, but the latest studies point at an important role of the triplet ligand field states as intermediate in the photocycle.^{10,14}

Whereas many experiments on spin crossover complexes are performed in solid state materials, most of the measurements on $[\text{Fe}(\text{bpy})_3]^{2+}$ are performed in solution. This eliminates any possible cooperative effect on the spin crossover properties and greatly facilitates the accurate theoretical treatment of the system, although one has to include the effect of the solvent on the electronic structure of the complex to ensure a correct description of the properties. Most theoretical studies of the electronic structure of $[\text{Fe}(\text{bpy})_3]^{2+}$ use the experimental low-spin structure or a geometry optimized with density functional theory (DFT) in vacuum. In both cases, the complex is highly symmetric in its low-spin configuration and transforms as the D_3 symmetry group. The three-fold rotation axis makes the three bipyridine ligands strictly equivalent and all Fe–N distances equal. As long as the ligand field states are concerned, this restriction does not have a large influence on the description. The quintet state shows a small Jahn-Teller distortion which results in an energy lowering not larger than 250 cm^{-1} .¹⁵ However, the situation is quite different when the MLCT excitations are considered. Due to the symmetry restrictions, the electron that is transferred from the metal to the ligands in the MLCT excitation is delocalized over the three ligands. This is probably not the most accurate description of the MLCT state as manifested in the study of the electronic structure of the related $[\text{Ru}(\text{bpy})_3]^{2+}$ complex. This complex

has a long-lived $^3\text{MLCT}$ state (≈ 500 ns), which is populated on a femtosecond scale by an intersystem crossing with the $^1\text{MLCT}$.¹⁶ Molecular dynamics simulations of the $^3\text{MLCT}$ state show that the electron is delocalized over the three ligands when the simulations are done in gas-phase, while it is localized on one or two ligands when the simulation is performed in solution, in line with the conclusions derived from spectroscopic measurements.¹⁷

A static, symmetric treatment of the electronic structure of $[\text{Fe}(\text{bpy})_3]^{2+}$ gives a reasonably precise description of the experimental absorption spectrum. In addition to the intense peaks at high energies ascribed to ligand-centered excitations, the general features of the MLCT band are also reproduced. This band has both contributions from singlet and triplet states, where the latter mainly contribute on the low-energy side. However, it was also recognized that the onset of the calculated MLCT absorption band is shifted to higher energies by about 0.25 eV in comparison to experiment.^{2,8} Computational parameters such as the active space and the size of the one-electron basis set play a very important role in the determination of the high-spin low-spin energy difference, but were shown to be less critical for accurate vertical excitation energies. The inclusion of solvent effects by a polarizable continuum model (PCM) hardly affects the excitation energy of the MLCT states.¹⁸ This weak effect of the solvent is easily explained by the fact that the dipole moment of the ground and excited MLCT states is (close to) zero if the extra electron on the ligand is delocalized over the three ligands in a symmetric way. In such a case the solvent polarization, if present at all, is equal for both states. Hence, the mismatch between the experimental and theoretical onset of the MLCT band might be caused by the delocalization of the transferred electron imposed by the symmetric structure. To verify this hypothesis we perform Car-Parrinello molecular dynamics (CPMD) simulations¹⁹ of $[\text{Fe}(\text{bpy})_3]^{2+}$ in water and select 20 snapshots along the simulation to calculate the relative energies of the ligand field and MLCT states of different spin coupling. The structure of the complex at the different snapshots shows a certain degree of distortion due to the thermal motion and the interaction with the water molecules of the solvent. Since the D_3 symmetry is lost, the calculation of the excitation energies at these snapshots and the analysis of the wave function can be of help to analyze the effect of localization of

the transferred electron on the character and relative energy of the MLCT states.

We restrict our study not only to the absorption spectrum of $[\text{Fe}(\text{bpy})_3]^{2+}$ and the onset of the MLCT band, but we also obtain valuable information about the relative energies of other states that are possibly populated along the deactivation path of the $^1\text{MLCT}$ in the LIESST process. The static description shows important gaps between possible intermediate states when scanning the Fe–N distance. In the CPMD simulations all classical vibro-rotational degrees of freedom are sampled, and hence, by calculating the energy of all the relevant electronic states on a representative sample of snapshots, one can see whether these gaps vanish in some specific conformations of the complex.

2 Computational information

The two-step procedure that we follow here for calculating the optical absorption spectrum including the effect of the thermal motion has been tested before for the ionic insulator NiO and a cytosine molecule dissolved in water.^{20,21} It starts with a CPMD simulation of the whole system imposing periodic boundary conditions on a (large) unit cell. Subsequently, excitation energies and oscillator strengths are calculated with accurate quantum chemical methods on a selection of snapshots to construct the *ab initio* absorption spectrum of the complex. The results are represented in a density estimation with Gaussian kernel functions of variable bandwidth (*bw*), which uses the oscillator strength of each transition to weight their contribution to the overall spectrum.

2.1 Molecular Dynamics simulation: The CPMD simulation was performed in a box of length 21 Å, containing one $[\text{Fe}(\text{bpy})_3]^{2+}$ complex, 298 water molecules and 2 Cl^- ions as in the previous calculations of Lawson Daku and Hauser.²² The core electrons are described by Troullier-Martins normconserving pseudo-potentials.²³ The electronic potential was calculated by means of the BLYP density functional^{24,25} using a plane waves basis set with a cut-off of 80 Ry. The system was first equilibrated at 300 K and then maintained at a steady temperature with a Nosé-Hoover chain thermostat.²⁶ All hydrogen atoms are deuterium isotopes to avoid the higher frequency

hydrogen stretching and be able to use a relatively large fictitious electron mass of $\mu = 700$ a.u., which combined with a time step of 0.097 fs ensures the proximity to the Born-Oppenheimer potential surface during the simulation. The MD simulations were carried out with the cpmd software²⁷ version 3.15 and the trajectory of the low-spin state was followed for 1.5 ps.

This simulation time is much shorter than in the calculations of Lawson Daku and Hauser, but the six Fe–N distances and the average bond distance printed in Fig. 1 show a similar distribution as the one obtained for the longer simulation. The average Fe–N bond length during the molecular dynamics is 1.977 Å, which is in very good agreement with the crystallographic measurement of 1.967 Å at 293 K.²⁸ The variation of the Fe–N bond lengths spans from 1.90 Å to 2.05 Å, completely covering the minimum of the LS state and a large part of its surroundings. This range of distortion appears to be sufficient to extract a representative sample of conformations from the MD trajectory and explore the classically accessible LS state at 300 K.

Figure 2 shows the thermal distribution of the twelve N–Fe–N’ angles along the Car-Parrinello MD simulation. Two main types of N–Fe–N’ angles can be observed on the thermal distribution, the bipyridine bite angle and the inter ligand angles. The differences between the metal–ligand bond angles of the $[\text{Fe}(\text{bpy})_3]^{2+}$ complex is in line with the experimental distorted octahedral environment of Fe(II). The average value of the bite angle along the MD trajectory is 81.4°, whereas the measured bite angle is 81.3°.²⁸ The inter ligand angles show a wider range of values, and two main regions can be distinguished at 88 - 89° and $\sim 95^\circ$, which correspond to the two different inter ligand angles of the D_3 structure. Finally, the mean value of the three N–Fe–N’ angles of the opposed Fe–N bonds is 173.2°.

2.2 *Ab initio* calculations: We calculate the electronic structure of the $[\text{Fe}(\text{bpy})_3]^{2+}$ complex extracted from the 20 snapshots along the CPMD trajectory with the complete active space second-order perturbation theory²⁹ (CASPT2) as implemented in the quantum chemistry code Molcas 7.³⁰ The snapshots were chosen equidistantly along the whole trajectory and provide a representative set of geometries. Test calculations on the previously studied systems showed that using more conformations does not change the main features of the calculated absorption spectrum and only lead to

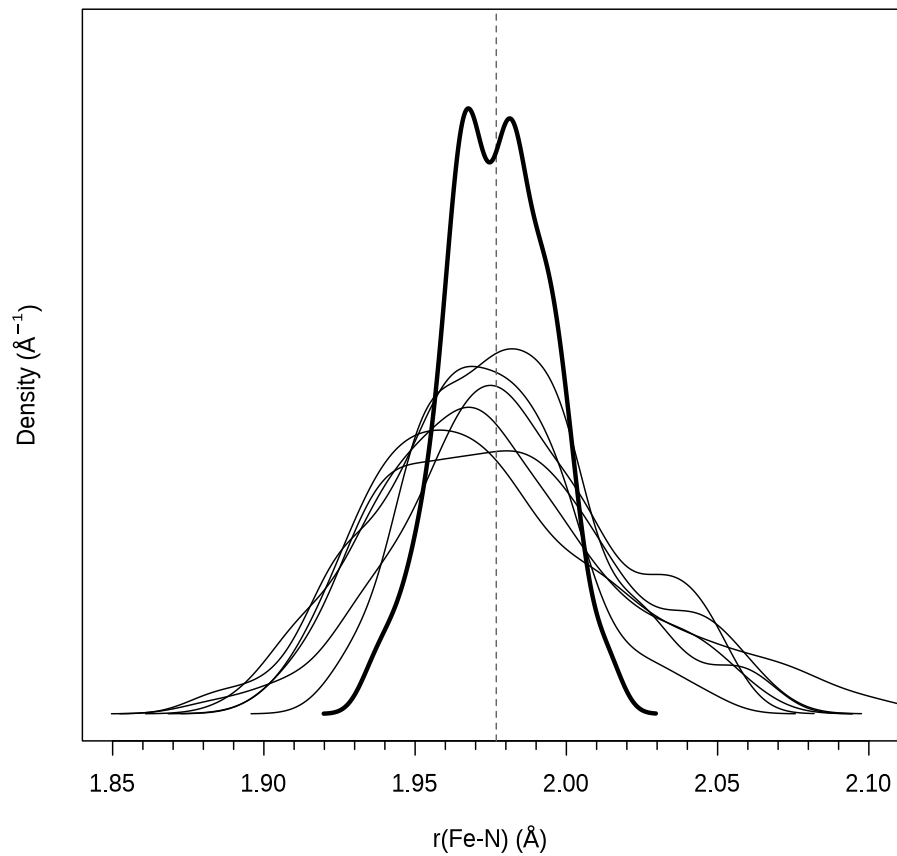


Figure 1: Thermal distribution of the six Fe–N bond lengths of the $[\text{Fe}(\text{bpy})_3]^{2+}$ complex resulting from the MD simulation. Each bond is represented by a thin line and the average of the six bonds by the thick line. The mean value of the average Fe–N bond along the simulation is 1.977 Å (dashed line).

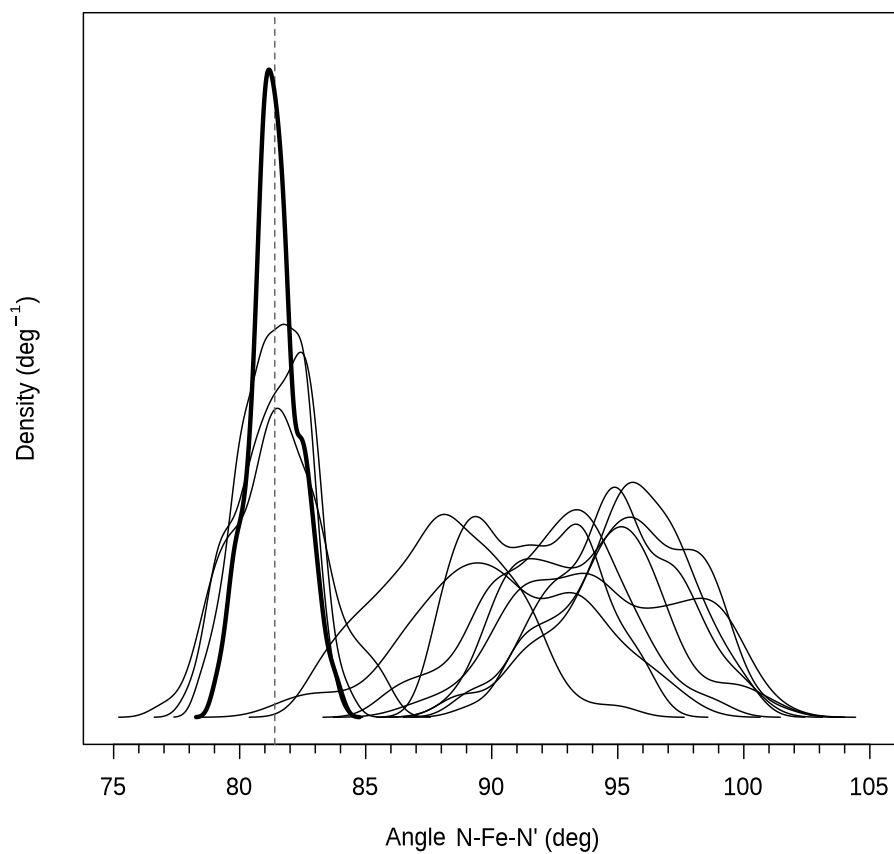


Figure 2: Thermal distribution of the twelve N–Fe–N' angles of the $[\text{Fe}(\text{bpy})_3]^{2+}$ complex resulting from the MD simulation. Each angle is represented by a thin line. The average of the three bite angles of the bpy ligand is represented by a thick line. The mean value of the average three N–Fe–N' bite angles along the simulation is 81.4° (dashed line).

smoother curves.³¹

We follow as close as possible the computational setup used in our previous studies of the complex.^{8,10} However, the loss of all the symmetry elements approximately doubles the computational effort and we decided to reduce the size of the one-electron basis set on the Fe atom to (6s,5p,4d,2f) functions. The very extended basis set used previously is essential to obtain reliable estimates of the HS-LS energy difference, but the requirements are less critical for vertical excitation energies. The basis set for the remaining atoms is kept as in previous works: N (4s,3p,1d); C (3s,2p); and H (2s). All the basis sets are of the ANO-RCC type.^{32,33}

The zeroth-order wave function for the CASPT2 calculation is obtained with the complete active space self-consistent field³⁴ (CASSCF) method. The active space has 10 electrons in 13 orbitals. These orbitals can be characterized as five Fe-3d orbitals, five Fe-4d like orbitals that account for the double shell effect,³⁵ two N σ orbitals directed along the Fe-N bonds, and one π^* orbital to allocate the electron on the bipyridine ligand(s) upon excitation. The study was not limited to excited singlet states, but we also calculated the relative energies of all the low-lying triplet and quintet states of ligand-field or MLCT character. We have calculated 12 singlets, 26 triplets and 12 quintets at each snapshot; in total 1000 states before considering spin-orbit coupling and 3000 states when spin-orbit coupling is taken into account. The amount of states computed for each spin multiplicity has been chosen to obtain spectra that span over ~ 4 eV of energy in average. The oscillator strength of the different transitions was calculated by the state-interaction module of Molcas with and without spin-orbit coupling³⁶ to pin-down the contribution of the triplet states to the MLCT band.

The CASPT2 calculations were done with the standard choice of the zeroth-order Hamiltonian (IPEA=0.25 Hartree) and an imaginary level-shift of 0.2 Hartree to avoid intruder state problems. All electrons were included in the second-order treatment of the correlation effects, except the deep core electrons Fe-1s²,2s²,2p⁶, C-1s² and N-1s². Static solvent effects were evaluated with the polarizable continuum model for two configurations extracted from the MD simulation.^{37,38}

3 Results

The earlier CPMD simulations on $[\text{Fe}(\text{bpy})_3]^{2+}$ and $[\text{Ru}(\text{bpy})_3]^{2+}$ showed that the complex is enclosed in a cage of water molecules.^{16,22} In the case of the LS state of the Fe complex, the average number of water molecules in this first coordination sphere of the complex was determined to be 17. Our simulations point in the same direction. Along the different snapshots, one can clearly observe a cage-like structure of water molecules, but the simulation time seems to be a little short to accurately determine the average number of water molecules that form the cage. However, the CPMD simulation in itself is not the main subject of this work, and as shown in the previous section, the simulation is long enough to generate a representative sample of snapshots with variations in bond distances and angles of similar magnitude as in the longer simulations reported in Ref. 22.

3.1 Analysis of the excited states: The closed and open circles shown in Figure 3 are the raw data obtained from the CASPT2 calculations on the twenty snapshots. The horizontal coordinate represents the excitation energy of the different transitions and the vertical axis indicates the intensity of the transition on a logarithmic scale. The closed circles are obtained from the calculations that neglect spin-orbit coupling and therefore only contain the singlet states. The open circles represent the results after taking into account spin-orbit coupling, which lifts the degeneracy of the levels with different M_S values and introduces a certain degree of spin mixing. Therefore, transitions to states that are dominated by triplet or quintet spin coupling are not completely spin-forbidden and have a non-zero oscillator strength. The solid black and grey lines are the representation of the raw data as density estimation with Gaussian kernel functions and can be interpreted as an *ab initio* representation of the onset of the lowest optically allowed band in the absorption spectrum of $[\text{Fe}(\text{bpy})_3]^{2+}$.

More information about the calculated absorption band requires an analysis of the wave function to determine the character of the excited states in the first place. Given the large number of data points, a full analysis of the multiconfigurational wave function is out of the question and a simple, semi-automatic criterion has to be found. For this purpose, we analyze first the twelve lowest excited singlet states of one of the

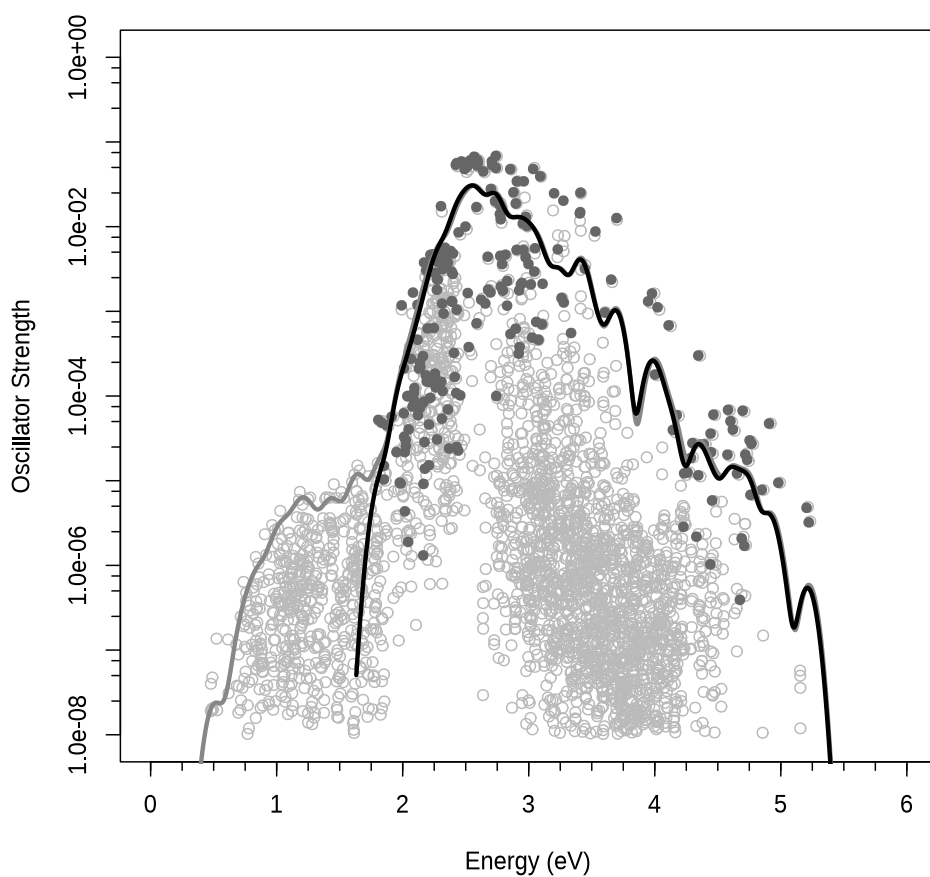


Figure 3: Absorption spectrum of LS $[\text{Fe}(\text{bpy})_3]^{2+}$ on a logarithmic scale calculated with CASPT2 from 20 snapshots along a 1.5 ps CPMD trajectory. Closed circles are the raw data considering singlet excitations only, the open circles are obtained taking into account spin-orbit coupling with singlet, triplet and quintet states. The two lines represent the spectrum as a density estimation with Gaussian kernel functions ($bw = 0.055$ eV) of the raw data.

Table 1: Analysis of the CASSCF wave function for the twelve lowest singlet states in one of the snapshots of the CPMD simulation. Natural occupation numbers of the active orbitals are given for the first root and changes to these for the other roots. The charge on Fe is calculated with the LoProp approach,³⁹ the population of the atomic Fe-3d orbitals is calculated with Mulliken population analysis. The dipole moment μ is calculated as the expectation value of the CASSCF wave function and the states are ordered by the CASSCF relative energy ΔE .

Root	Natural occupation numbers						ΔE	
	Fe-3d(t_{2g})	Fe-3d(e_g)	L- π^*	q(Fe)	d-count	μ (D)	CASSCF	CASPT2
1	5.876	0.081	0.031	1.04	6.38	0.244		
2	-0.953	0.948	0.004	1.18	6.26	0.571	2.168	2.090
3	-0.951	0.949	-0.004	1.18	6.27	0.394	2.443	2.393
4	-0.953	0.949	-0.004	1.18	6.27	0.542	2.558	2.524
5	-0.982	0.300	0.723	1.33	6.11	6.134	3.241	2.082
6	-0.961	0.051	0.948	1.38	6.05	8.376	3.445	2.240
7	-0.963	0.260	0.744	1.30	6.14	5.517	3.555	2.421
8	-1.048	0.992	0.062	1.21	6.24	0.906	3.853	3.261
9	-1.071	1.062	0.004	1.20	6.26	0.190	3.895	3.445
10	-1.089	0.707	0.396	1.24	6.22	1.666	4.113	3.411
11	-1.907	1.905	-0.005	1.32	6.17	0.599	4.739	4.718
12	-1.882	1.875	-0.002	1.32	6.16	0.317	4.935	4.733

snapshots in some detail to establish a simple way to identify the excited states.

The most rigorous way to analyze the character of the states in a CASSCF calculation is to identify the character of the active orbitals and determine the natural occupation numbers of these. As long as the orbitals are reasonably localized either on Fe or on the ligands, the leading electronic configuration of the wave function can be determined and one can easily identify the character of the excited states by looking at the changes in the natural occupation numbers. Table 1 shows the natural occupation numbers of the active orbitals in the ground state and the changes in the lowest 11 excited singlet states in one of the snapshots (ordered by the CASSCF energy). The

ground state has nearly six electrons in the Fe-3d(t_{2g})-like orbitals. The wave function is however not strictly monoconfigurational and has small contributions from electronic configuration with electrons in the Fe-3d(e_g)-like and ligand- π^* orbitals. State 2, 3, 4 are ligand field states in which one electron has been excited from a t_{2g} -like orbital into an e_g -like orbital of the Fe-3d shell. In a strict octahedral surrounding, this would correspond to the three degenerate components of the ${}^1T_{1g}$ state. The next three states are dominated by the electronic configuration in which one electron is transferred from a Fe-3d(t_{2g})-like orbital to a π^* orbital on the ligand, that is, three 1MLCT states with some contribution of the $t_{2g} \rightarrow e_g$ metal-centered excitations for state 5 and 7. States 8-10 are again ligand-field states with an Fe-3d($t_{2g}^5 e_g^1$) configuration, the three components of the ${}^1T_{2g}$ state in O_h symmetry. The last two states listed in the Table are excited states that involve double electron replacements in the Fe-3d shell.

Although this analysis rigorously identifies the character of the electronic states, a simpler strategy is required to analyze all the data generated at the twenty snapshots. For this purpose, we compare the outcomes of the analysis of the natural occupation numbers with the charge on Fe ($q(\text{Fe})$),³⁹ the number of electrons in the Fe-3d shell (d-count) and the dipole moment of the different electronic states. These quantities are easily extracted from the output files and could in principle give a fast identification of the electronic states. It is expected that both the net charge on Fe and the number of d-electrons change by a considerable amount when an electron is transferred from the Fe-3d orbitals to the ligand- π^* orbital. However, as can be seen in Table 1, neither quantities is capable of distinguishing between metal centered and MLCT states in a clear way. The changes of ~ 0.2 electron in q and the d-count are too small to be reliable for identification. On the other hand, we do observe a markedly different dipole moment in the states that have been identified as MLCT in comparison to the ground state and the other ligand-field states. The size of the dipole moment is approximately what can be expected for the separation of two opposite charges by 2.8 Å, the distance from the Fe ion to the midpoint of the C-C bond that connect the two rings of the bipyridine ligand.

In the symmetric structure no such dipole moments were observed for the MLCT

states due to the fact that the electron on the ligand is delocalized over the three equivalent bipyridines and the dipole moment vanishes. However, as can be seen in Fig. 4, the transferred electron localizes on one of the ligands in the asymmetric structures considered here. Fig. 4 shows the superposition of the ligand π^* orbital in the active space of all twenty snapshots. All these orbitals are very similar and well localized on one single bipyridine ligand of the complex. The image is generated by centering the twenty orbital images on the midpoint of the C–C bond and subsequently orienting the $[\text{Fe}(\text{bpy})_3]^{2+}$ complexes as to maximize the overlap between the different conformations.

Several attempts have been made to converge the wave function with an active space that includes π^* orbitals on all three ligands as done previously for the symmetric structure.^{8,10} However, the loss of symmetry induced by the thermal motion renders the three bipyridines to be non-equivalent. The orbital energies of the lowest unoccupied π^* orbitals are different, and hence, the localization on the ligand with the lowest-lying π^* orbital competes with the energy gain obtained by the delocalization of the electron over three ligands. Unless we include very high roots in the state-average CASSCF calculations, the π^* orbitals with higher orbital energies remain unoccupied and the wave function cannot be optimized with these orbitals in the active space. This shows that there is no delocalization over the three π^* orbitals in the lower MLCT states and that the MLCT states in which the higher-lying π^* orbitals would be occupied are high in energy. Moreover, even though all three bipyridine ligands are non-equivalent in each conformation, they are equivalent in the ensemble of conformations since they experience the same degree of distortions during the simulation. Hence, there is no gain in including one π^* orbital per ligand in the active space, as the span of energies of the MLCT obtained for each one of them would be very similar.

The localized character of the ligand orbital in all conformations strongly advocates for a scenario in which the excitation from ground state to $^1\text{MLCT}$ state involves only one of the bipyridine groups. The alternative description of a symmetric, delocalized excited MLCT state that induces a distortion accompanied by the localization of the electron on one of the ligands seems less plausible. This would require a (nearly) symmetric geometry with (nearly) identical bipyridine ligands. Such conformations may

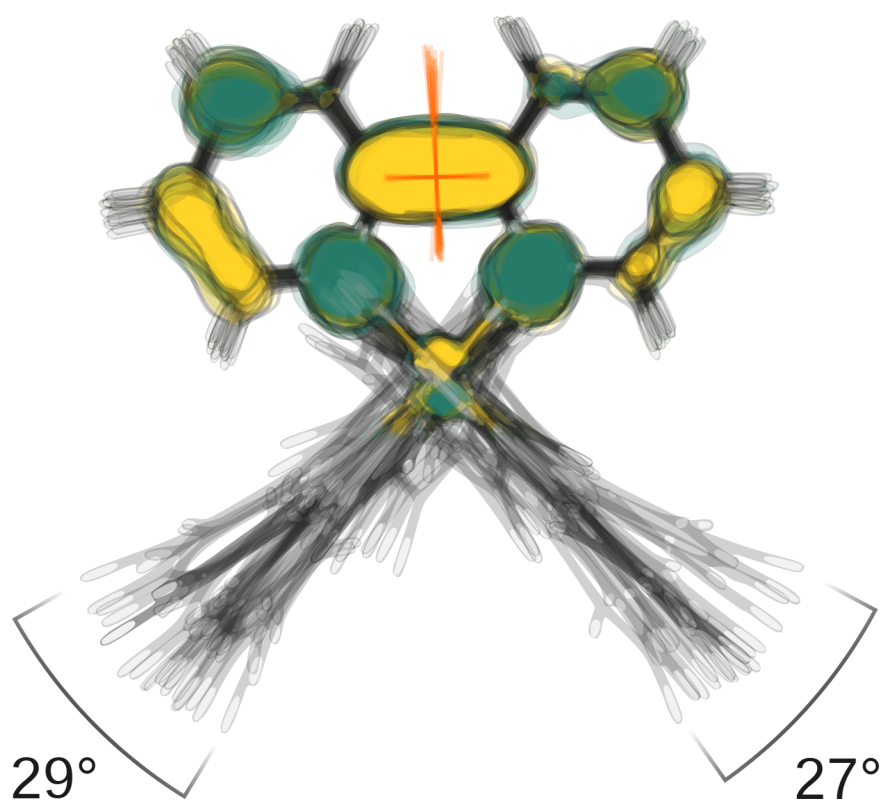


Figure 4: Graphical representation of the ligand π^* active orbital obtained for each one of the twenty $[\text{Fe}(\text{bpy})_3]^{2+}$ conformations. All structures are first centered at the midpoint of the C-C bond (red cross) and then oriented to maximize their overlap. The positive/negative parts of the orbital are in yellow/green color.

be frequent at low temperatures, but the CPMD simulations at 300 K show that in almost all cases the complex has non-equivalent ligands. Similar conclusions were derived from the molecular dynamics simulation on the $^3\text{MLCT}$ surface of $[\text{Ru}(\text{bpy})_3]^{2+}$.¹⁷ In that complex, the $^1\text{MLCT}$ is rapidly converted to a long living $^3\text{MLCT}$ state and the calculations show that the electron can hop from one ligand to the other before the $^3\text{MLCT}$ state decays to the initial ground state. This hopping mechanism is less relevant for the $[\text{Fe}(\text{bpy})_3]^{2+}$ complex since the $^3\text{MLCT}$ state is very short living and decays within less than 200 fs to the metastable HS state.^{1,10,13}

3.2 Decomposition of the MLCT band: Because the logarithmic scale used in Fig. 3 could easily lead to misinterpretation of the importance of the spin states other than singlet, we first analyze the spectrum on a linear oscillator strength scale. Fig. 5 compares the results obtained with the ideal symmetric structure in Ref. 8 (in grey) and the present representation of the onset taking into account the effect of the thermal motion of the atoms (in black). The linear oscillator strength scale makes more clear that the absorption is strongly dominated by singlet excitations. The contribution of triplet states is most obvious on the lower side of the MLCT band, at approximately 0.2 eV lower energy than the maximum of the singlet absorption. The $^3\text{MLCT}$ states have the same electronic configuration as the singlet coupled CT states: $\text{Fe-}3d(t_{2g})^5\text{L-}(\pi^*)^1$ with two unpaired electrons (L=ligand). Therefore, the lower energy of the $^3\text{MLCT}$ state can be largely ascribed to the exchange interaction between these two unpaired electrons, which lowers the triplet energy by 2K with respect to the singlet. A value of K of 0.1 eV seems reasonable as it is intermediate between the larger K of ~ 1 eV, observed for unpaired electrons localized in atoms (Hund’s rule) and the smaller K values, on the order of 1-10 meV, of the direct exchange contribution to the magnetic coupling of paramagnetic transition metal ions connected by a diamagnetic bridge.

Both representations in Fig. 5 already show this difference between singlet and triplet states. The only important effect of the inclusion of the thermal motion, and hence the loss of the symmetry, is the shift of the excitation energies by 0.2 eV to lower energy. This brings the on-set of the MLCT band in better agreement with experimental data and repairs the overestimation found in previous works.^{8,18} It demonstrates

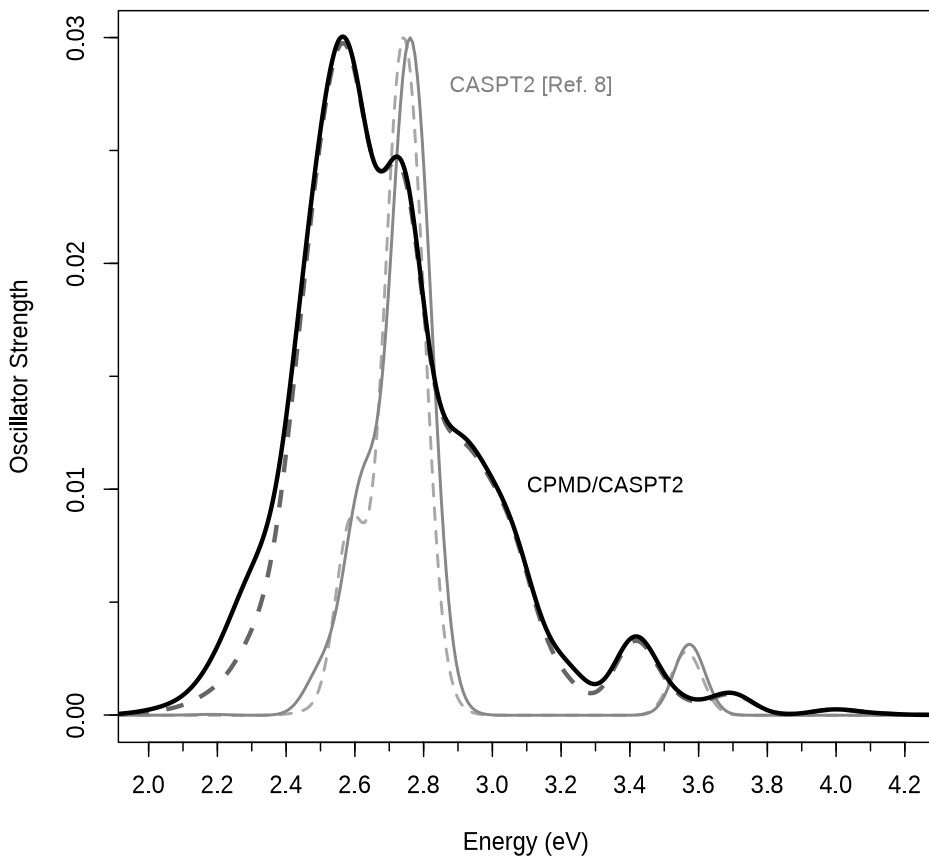


Figure 5: Absorption spectrum of LS $[\text{Fe}(\text{bpy})_3]^{2+}$ on a linear scale at the CASPT2 level. Absorption bands without spin-orbit coupling (singlets only, dashed lines) and with spin-orbit coupling (solid lines). The grey lines are calculated with the symmetric D_3 structure by associating a Gaussian function to each transition with a full width at half maximum of 0.15 eV, see Ref. 8. The black lines represent the density estimation with Gaussian kernel functions ($bw = 0.060$ eV) resulting from the combined CPMD/CASPT2 calculation.

that the localization of the electron on one of the bipyridine ligands lowers the MLCT excitation energy with respect to the delocalized representation obtained in the symmetric structure. The metal centered states do not show this energy lowering. The average excitation energies obtained from the distorted structures is roughly the same as those calculated for the symmetric structure.

Based on the analysis of the previous section, the MLCT states were identified by their larger dipole moment with respect to the ligand-field states. This automatically brings up the question of the effect of the solvent. The polarization of the solvent induced by changes of the dipole moment when the complex is excited into one of these MLCT state can affect the excitation energies. The polarized continuum model has become the standard way to model solvent effects on geometries and excitation energies of solutes and provides reasonably accurate results at a very moderate computational cost. More accurate representations of the solvent with explicit water molecules go far beyond the present computational possibilities, since many molecules have to be included in the computational model to obtain a balanced description. One should at least consider the 17 water molecules intercalated between the bipyridine ligands as found in the simulations of Lawson Daku and Hauser.²² Therefore, we have used the PCM model to check the effect of the solvent on the excitation energy of the ¹MLCT states in two conformations; one with relatively low excitation energies and the second with higher-lying MLCT states. We have limited ourselves to these two conformations, because the convergence in the CASSCF step of the calculation is significantly slower when PCM is used. As expected, the excitation energy of the ligand field states is virtually the same in gas phase and in the PCM representation of the water-solvated complex. On the other hand, we do observe a solvent effect for the ¹MLCT states. The excitation energy of all six states considered in this check (three per conformation) become red-shifted by 0.1 eV at most. Based on the similarity of the dipole moment of the MLCT states in the other conformations, we expect this lowering to happen for all MLCT states. Hence, the 0.2 eV lowering due to the localization and the 0.1 eV caused by the polarization of the solvent can be added to roughly 0.3 eV, which is close to the mismatch of 0.25 eV that was previously found in the gas-phase calculations on the symmetric structure.

Having established that the combination of CPMD with single-point CASSCF/CASPT2 calculations results in more accurate excitation energies for the lowest absorption band of $[\text{Fe}(\text{bpy})_3]^{2+}$, we now proceed with the analysis of the raw data. For this purpose, we return to the logarithmic oscillator strength scale and decompose the calculated absorption band in different contributions depending on the spin coupling of the unpaired electrons and the character of the excitation as shown in Fig. 6. We use the dipole moment of the final state to establish the character of each excitation. As a rule of thumb, we assign all excitations with a dipole moment in the final state lower than 1.5 D as metal-centered excitations and states with a dipole moment larger than 4.0 D as MLCT states (see Tab. 1). The transitions that do not fit this criteria are excitations of mixed character, involving multiple intra-metallic d-d and/or MLCT components.

The combination of all ligand field transitions constitutes the only contribution to the overall spectrum in the 0-2 eV range. This band is depicted in Fig. 6 with a thick blue line. To make contact with the symmetric structure, we have decomposed the ligand field band in transitions to the low-lying T states found in the O_h system. Each band filled in blue corresponds to one of such d-d transitions. Those excitations are dipole forbidden in a strict octahedral coordination of Fe, but they gain a weak intensity due to the loss of symmetry induced by the thermal motion. In addition, the excitations to the triplet and quintet states (${}^3T_{1g,2g}$ and ${}^5T_{2g}$ in O_h) are spin forbidden and thus, even less intense. The variation of the excitation energy of the 5T between 0.5 eV and more than 2 eV is strongly related with the average Fe-N distance: the longer this distance, the lower the 5T transition energy. The Fe-3d($t_{2g}^4 e_g^2$) electronic configuration of the quintet is stabilized with increasing Fe-N distance, whereas the singlet ground state is destabilized at larger distances. Similar, but less strong correlations are also found for the 3T and 1T states with $t_{2g}^5 e_g^1$ configurations.

The MLCT transitions span from 2 eV to beyond 4 eV, forming the band depicted with a thick red line. The MLCT band contains basically four contributions. The largest one is due to the ${}^1\text{MLCT}$ transitions and dominates the absorption spectrum. At the low energy side, a shoulder appears arising from states that are dominated by configurations with triplet coupling. These states gain some intensity due to the

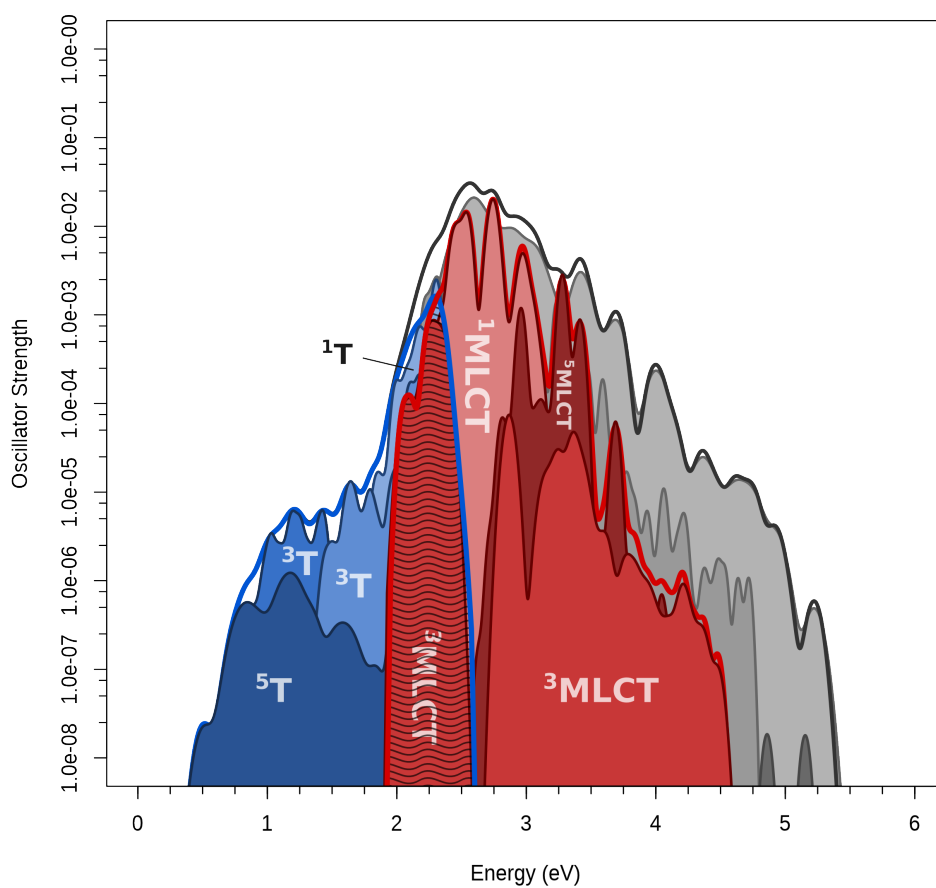


Figure 6: Decomposition of the absorption band on a logarithmic scale in ligand field (blue) and MLCT (red) contributions. The grey peaks are due to double excitations of mixed character. From light to dark, the peaks are separated in singlet, triplet and quintet contributions. The combined contributions of all ligand field bands and all MLCT bands are depicted with blue and red thick lines, respectively. The zone of overlap between these bands is marked with a ripple pattern.

admixture of singlet configurations after treating the spin-orbit coupling. At higher energy, starting around 2.7 eV, a second ${}^3\text{MLCT}$ band appears. Most of the states that contribute to this band have a $\text{Fe-3d}(t_{2g}^4 e_g^1)\text{L-}\pi^*1$ configuration, arising from a combined MLCT and ligand field excitation. The contribution of the quintet states starts at approximately 2.6 eV and extends along the same range of energies as the ${}^3\text{MLCT}$ band. The overlap of the ${}^5\text{MLCT}$, ${}^3\text{MLCT}$ and ${}^1\text{MLCT}$ bands in Fig. 6 may lead to the conclusion that in some cases these states become close in energy allowing the deactivation via the ${}^5\text{MLCT}$ states as suggested in the literature. However, a more detailed analysis shows that ${}^5\text{MLCT}$ states of low energy occur in conformations where the ${}^{1,3}\text{MLCT}$ states are also on the low energy side of the band. The difference between the lowest ${}^{1,3}\text{MLCT}$ and lowest ${}^5\text{MLCT}$ states is reasonably constant, approximately 1 eV and in none of the conformations the order is inverted, as shown in the upper part of Figure 7.

On the contrary, the mechanism involving the deactivation via triplet ligand field states is reinforced by the present results. The singlet, triplet and quintet states with a dominant ligand field character undergo an increase of intensity of approximately one order of magnitude beyond 2.0 eV energies. In the 2.0-2.5 eV region, the ligand field and MLCT bands overlap (ripple pattern in Fig. 6) and hence, the ligand field states gain a charge transfer component increasing their intensity. In that region of overlap, the mixture of states could favour both the direct ${}^3\text{MLCT}\rightarrow{}^3\text{T}_2\rightarrow{}^5\text{T}$ deactivation and the pathway involving both triplet ligand field as proposed in Ref. 10. The ${}^3\text{MLCT}$ band partially overlaps with the ${}^3\text{T}_2$ band, which in turn overlaps with the lower ${}^3\text{T}_1$ band and with the ${}^5\text{T}$ band.

To close this section, we make two more remarks. In the first place, the states at higher energy are either strongly mixed of character and therefore difficult to label or arise from double electron replacements in the Fe-3d shell as the eleventh and twelfth root listed in Table 1. Secondly, it should be kept in mind that the active space only includes one ligand π^* orbital, and hence, we only sample the lower part of the MLCT manifold. A description with more (higher-lying) π^* orbitals in the active space would broaden the absorption on the high-energy side of the band and improve the comparison with experiment concerning the shape of the MLCT band. It will,

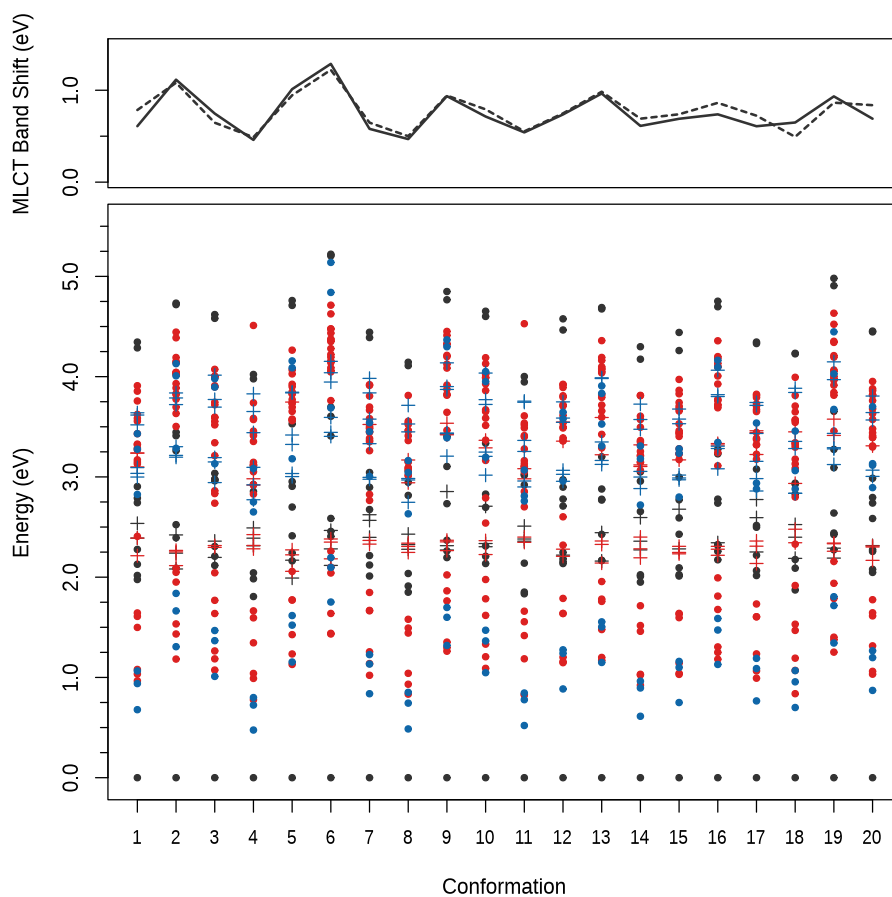


Figure 7: Relative energies of the ligand field (dots) and MLCT states (crosses) in the twenty conformations. All calculated transitions to singlet excited states (black), triplet states (red) and quintet states (blue) are included. The upper part shows the energy difference between the lowest quintet and singlet (solid line) or triplet (dashed line) MLCT states.

however, not move the on-set of the MLCT band, neither affect the discussion of the likeliness of the different deactivation mechanisms, since this involves basically the lower MLCT states and the whole range of ligand-field states, which are extensively sampled.

4 Conclusions

The thermal motion of the ions continuously distorts the symmetric D_3 structure of $[\text{Fe}(\text{bpy})_3]^{2+}$ in its LS state. This has important consequences for the theoretical description of the electronic structure of the complex and offers new insights towards a complete description of the deactivation process of the excited singlet state in the LS to HS spin crossover induced by light. In the first place, we have shown that the vertical excitation in the Franck-Condon region implies the transfer of an Fe-3d electron to one of the bipyridine ligands (Fig. 4), instead of the delocalized picture that emerges from the description with the symmetric structure. This localization on one ligand is accompanied by an energy lowering of 0.20 eV (Fig. 5) and together with the solvent effect of approximately 0.1 eV, this shifts the on-set of the MLCT band to the same energy as experimentally found.

The decomposition of the absorption peak in contributions from singlet, triplet and quintet states (Fig. 6) reveals that the triplet states make the largest contribution at the low energy side of the band, approximately 0.2 eV below the maximum of the singlet MLCT states. Furthermore, we have found no conformation for which the MLCT state with quintet spin coupling is lower in energy than the singlet or triplet states. This definitely rules out any possibility of a double intersystem crossing in the MLCT manifold as suggested in the literature.⁹ On the other hand, the energy lowering of 0.3 eV of the MLCT band brings it closer to the triplet ligand field states and favors a fast deactivation to the quintet state. We observe that in some conformations the two triplet ligand field states (${}^3\text{T}_2$ and ${}^3\text{T}_1$ in an octahedral complex) have nearly identical energies and also overlap with the ${}^5\text{T}$ band. This indicates that certain distortions bring these ligand field states close in energy, opening the possibility for a fast decay as experimentally observed.^{3,13,14}

Acknowledgments: Financial support has been provided by the Spanish Administration (CTQ2011-23140 and CTQ2012-30751), the Generalitat de Catalunya (2009SGR462, 2014SGR97 and Xarxa d'R+D+I en Química Teòrica i Computacional, XRQTC) and the European Union (COST Action ECOSTBio CM1305).

References

- [1] J. K. McCusker, K. N. Walda, R. C. Dunn, J. D. Simon, D. Magde, and D. N. Hendrickson, *J. Am. Chem. Soc.* **115**, 298 (1993).
- [2] W. Gawelda, A. Cannizzo, V.-T. Pham, F. van Mourik, C. Bressler, and M. Chergui, *J. Am. Chem. Soc.* **129**, 8199 (2007).
- [3] C. Bressler, C. Milne, V.-T. Pham, A. ElNahhas, R. M. van der Veen, W. Gawelda, S. Johnson, P. Beaud, D. Grolimund, M. Kaiser, C. N. Borca, G. Ingold, R. Abela, and M. Chergui, *Science* **323**, 489 (2009).
- [4] C. Bressler and M. Chergui, *Annu. Rev. Phys. Chem.* **61**, 263 (2010).
- [5] A. Cannizzo, C. J. Milne, C. Consani, W. Gawelda, C. Bressler, F. van Mourik, and M. Chergui, *Coord. Chem. Rev.* **254**, 2677 (2010).
- [6] H. Cho, M. L. Strader, K. Hong, L. Jamula, E. M. Gullikson, T. K. Kim, F. M. F. de Groot, J. K. McCusker, R. W. Schoenlein, and N. Huse, *Faraday Discuss.* **157**, 463 (2012).
- [7] M. Chergui, *Dalton Trans.* **41**, 13022 (2012).
- [8] C. de Graaf and C. Sousa, *Chem. Eur. J.* **16**, 4550 (2010).
- [9] M. van Veenendaal, J. Chang, and A. J. Fedro, *Phys. Rev. Lett.* **104**, 067401 (2010).
- [10] C. Sousa, C. de Graaf, A. Rudavskiy, R. Broer, J. Tatchen, M. Etinski, and C. M. Marian, *Chem. Eur. J.* **19**, 17541 (2013).
- [11] S. Iuchi, *J. Chem. Phys.* **136**, 064519 (2012).

- [12] S. Iuchi, *J. Chem. Phys.* **140**, 024309 (2014).
- [13] C. Consani, M. Premont-Schwarz, A. ElNahas, C. Bressler, F. van Mourik, A. Cannizzo, and M. Chergui, *Angew. Chem. Int. Ed.* **48**, 7184 (2009).
- [14] W. Zhang, R. Alonso-Mori, U. Bergmann, C. Bressler, M. Chollet, A. Galler, W. Gawelda, R. G. Hadt, R. W. Hartsock, T. Krill, K. S. Kjær, K. Kubiček, H. T. Lemke, H. W. Liang, D. A. Meyer, M. M. Nielsen, C. Purser, J. S. Robinson, E. I. Solomon, Z. Sun, et al., *Nature* **509**, 345 (2014).
- [15] K. Pierloot and S. Vancoillie, *J. Chem. Phys.* **125**, 124303 (2006).
- [16] A. Cannizzo, F. van Mourik, W. Gawelda, G. Zgrablic, C. Bressler, and M. Chergui, *Angew. Chem. Int. Ed.* **45**, 3174 (2006).
- [17] M.-E. Moret, I. Tavernelli, M. Chergui, and U. Rothlisberger, *Chem. Eur. J.* **16**, 5889 (2010).
- [18] S. Saureu and C. de Graaf, *Chem. Phys.* **428**, 59 (2014).
- [19] R. Car and M. Parrinello, *Phys. Rev. Lett.* **55**, 2471 (1985).
- [20] A. Domingo, A. Rodríguez-Forteza, and C. de Graaf, *J. Chem. Theory Comput.* **8**, 235 (2012).
- [21] A. Domingo, A. Rodríguez-Forteza, M. Swart, C. de Graaf, and R. Broer, *Phys. Rev. B* **85**, 155143 (2012).
- [22] L. M. Lawson Daku and A. Hauser, *J. Phys. Chem. Lett.* **1**, 1830 (2010).
- [23] N. Troullier and J. L. Martins, *Phys. Rev. B* **43**, 1993 (1991).
- [24] A. D. Becke, *Phys. Rev. A* **38**, 3098 (1988).
- [25] C. T. Lee, W. T. Yang, and R. G. Parr, *Phys. Rev. B* **37**, 785 (1988).
- [26] S. Nosé, *J. Chem. Phys.* **81**, 511 (1984).
- [27] *CPMD; IBM Corp.: Endicott, NY, 1990; MPI für Festkörperforschung: Stuttgart, Germany, 1997.*

- [28] S. Dick, *Z. Krist.-New Cryst. St.* **213**, 356 (1998).
- [29] K. Andersson, P.-Å. Malmqvist, B. O. Roos, A. J. Sadlej, and K. Wolinski, *J. Phys. Chem.* **94**, 5483 (1990).
- [30] F. Aquilante, L. De Vico, N. Ferré, G. Ghigo, P.-Å. Malmqvist, P. Neogrady, T. B. Pedersen, M. Pitoňák, M. Reiher, B. O. Roos, L. Serrano-Andrés, M. Urban, V. Veryazov, and R. Lindh, *J. Comput. Chem.* **31**, 224 (2010).
- [31] *A. Domingo, Theoretical description of electronic excitations in extended systems: beyond the static material model, PhD Theses, University Rovira i Virgili, Tarragona (2011). URL: <http://www.tdx.cat/handle/10803/51760>.*
- [32] B. O. Roos, R. Lindh, P.-Å. Malmqvist, V. Veryazov, and P.-O. Widmark, *J. Phys. Chem. A* **108**, 2851 (2004).
- [33] B. O. Roos, R. Lindh, P.-Å. Malmqvist, V. Veryazov, and P.-O. Widmark, *J. Phys. Chem. A* **109**, 6575 (2005).
- [34] B. O. Roos, P. R. Taylor, and P. E. M. Siegbahn, *Chem. Phys.* **48**, 157 (1980).
- [35] K. Andersson and B. O. Roos, *Chem. Phys. Lett.* **191**, 507 (1992).
- [36] B. O. Roos and P.-Å. Malmqvist, *Phys. Chem. Chem. Phys.* **6**, 2919 (2004).
- [37] M. Cossi, V. Barone, R. Cammi, and J. Tomasi, *Chem. Phys. Lett.* **255**, 327 (1996).
- [38] E. Cancès, B. Mennucci, and J. Tomasi, *J. Chem. Phys.* **107**, 3032 (1997).
- [39] L. Gagliardi, R. Lindh, and G. Karlström, *J. Chem. Phys.* **121**, 4494 (2004).